OPEN ACCESS

Volume: 4

Issue: 1

Month: January

Year: 2025

ISSN: 2583-7117

Published: 25.01.2025

Citation:

Ausaf Ahmad Usmani, Pankaj Shrivastava, Shivendra Singh "Impacts of Fins on The Heat Transfer Characteristics in A Shell and Cone-Shaped Coil Heat Exchanger" International Journal of Innovations In Science Engineering And Management, vol. 4, no. 1, 2025, pp. 118–129.

DOI:

10.69968/ijisem.2025v4i1118-129

Examine the effect of various shape of absorber plate of solar air heater integrated with vortex generator

Kundan Kumar[1], Shivendra Singh[2], Dr. B. Suresh[3]

[1]Research Scholar, Department of Mechanical Engineering, Corporate Institute of Science & Technology, Bhopal
[2]Asst. Prof., Department of Mechanical Engineering, Corporate Institute of Science & Technology, Bhopal
[3]Prof. & HOD, Department of Mechanical Engineering, Corporate Institute of Science & Technology, Bhopal

Abstract

Solar energy is a noteworthy renewable energy source that may be used as a sustainable substitute for fossil fuels in many applications, including evacuated tube solar collectors, solar water heaters, and solar air heaters (SAHs). Among these, SAHs are widely utilized due to their simplicity and efficiency. In a solar air heater duct with rectangular vortex generators, this research examines the effects of various absorber plate configurations employing "computational fluid dynamics (CFD)". Heat transmission between the air and the absorber plate was examined using three different absorber plate geometries: corrugated, triangular, and trapezoidal. Additionally, variations in the geometric configurations of the triangular and trapezoidal ribbed absorber plates were considered. The air velocity was constant at 1.31 m/s in each instance, while "the absorber plate" was continually exposed to a heat flux of 815 W/m². The rate of heat transfer, outlet air temperature, temperature contours, pressure contours, velocity contours, and other critical performance metrics were investigated. The results indicate that heat transfer is significantly higher in SAH ducts with triangular and trapezoidal ribbed absorber plates compared to the corrugated plate. The maximum outlet air temperature of 325.83 K and a heat transfer rate of 595.44 W were observed in case 6, representing the highest values among all configurations studied. These results demonstrate how optimized ribbed designs may improve solar air heaters' thermal performance.

Keywords; Heat Flux, Triangular Ribs, Trapezoidal Ribs, Corrugated Absorber, Heat Transfer

INTRODUCTION

The Sun's radiation, which may produce heat, electricity, or chemical reactions, is known as "solar energy". There is much more solar energy that reaches Earth overall than is now required and will be required in the future [1]. The world's energy demands may be satisfied by this dispersed energy source if properly harnessed. In the twenty-first century, solar energy has become more and more popular as a renewable energy source because of its endless supply and non-polluting characteristics, in contrast to the limited availability of traditional energy sources "like coal, oil, and natural gas" [2][3]. In order to protect ecosystems, wildlife, and people, it is essential to reduce emissions of greenhouse gases and stop climate change. One renewable energy source which assists in achieve this goal is solar energy. In addition to lowering the amount of water needed to generate power, solar energy may also help host towns' ecology by managing storm and ground water, pollination, and sequestering carbon [4][5]. Sites for "ground-mounted photovoltaic (PV) and concentrated solar thermal power (CSP) systems" should be carefully chosen, planned, and maintained with respect for local species, ecosystems, water supplies, and soil [6][7]. In order to better understand the interactions between solar energy systems, animals, and ecosystems and to provide solutions that maximize advantages to the local ecosystems and host populations, the U.S. Department of Energy (DOE) funds research via its "Solar Energy Technologies Office (SETO)" [8].

Solar air heater

Solar energy, which may be captured and used in a variety of ways, powers “solar air heaters”. When the solar air heater's absorbing surface is contact with “the solar energy or the sun's irradiance”, its radiation is absorbed and transferred to the collecting system, which might be a fluid like water or air traveling through a tube [9]. Water is the most often utilised fluid. Even at temperatures below 0 degrees, the fluid within does not freeze [10]. Stiff roughness and a variety of shapes are applied to the bottom to improve heat transmission. One extremely important economic issue is that the thermal insulation on the sides and bottom keeps heat from escaping [11].

Non-Porous Type Solar Air Heater

The gap below the absorber plate is not where air flows in non-porous solar air heaters. Rather, it might flow behind or above the plate. The first kind involves direct air movement between the absorber plate and the transparent cover. The design's main drawback is the substantial quantity of heat lost to the environment due to the cover's ability to absorb the majority of the heat from the hot air passing over the absorber [12][13]. It is not advised to use this kind of air heater because of its inefficiency. A plate positioned parallel to the absorber itself in the more common non-porous kind creates a high aspect ratio path through "the absorber and the insulation" while allowing air to flow underneath the absorber [14]. Heat is better captured and retained by this design. The air stream that flows past the absorber plate on both sides lowers it in a different kind of non-porous air heater. The solar air heater's efficiency is significantly increased by this design.

Porous-Type Solar Air Heater

An ingenious gadget that makes use of microscopic pores or perforations in its absorber plate is a “porous type solar air heater”. The air passing through these tiny holes warms up when sunshine strikes the plate. The space or room that requires warming is subsequently filled with this hot air [12][15]. It functions similarly to an eco-friendly, intelligent heater that harnesses solar energy. The absorber plate is an effective method of capturing solar energy for heating because of the microscopic pores that enable air to travel through and heat up [16]. These kinds of solar air heaters are easy to use, environmentally friendly, and may save energy expenses. People may have a warm and comfortable area without depending entirely on electricity or other conventional heating techniques thanks to the “porous type solar air heater” [17][18].

OBJECTIVE

- Investigate the various design of absorber plate as like corrugate, triangular and trapezoidal shape attach to solar air heater.
- Investigate the outlet temperature, temperature distribution, pressure distribution and velocity distribution in air flow inside the duct.
- Examine the change in the design parameter of the triangular and trapezoidal ribs absorber plate.
- Examine the rate at which heat transfers through the solar air heater's absorber plate, which has various "corrugated, triangular, and trapezoidal ribs".

RESEARCH METHODOLOGY

Governing equation

The airflow within the "solar air heater duct" is controlled using the following formulas.

Steady-state continuity equation:

$$\frac{\partial}{\partial x_i}(\rho u_i) = 0$$

Incompressible and time-independent The Navier-Stokes equation:

$$\frac{\partial}{\partial x_i}(\rho u_i u_j) = -\frac{\partial P}{\partial x_i} + \frac{\partial}{\partial x_j}\left[\mu \frac{\partial u_i}{\partial x_j} + \frac{\partial u_j}{\partial x_i}\right] + \frac{\partial}{\partial x_i}(-\rho \acute{u_i} \acute{u_j})$$

In the direction of xi, i≠j, P, ρ, μ, ui, and u′i stand for pressure, fluid density, dynamic viscosity, and the mean and changeable components of velocity, respectively.

Energy formula

$$\rho c_p u_i \frac{\partial T}{\partial x_i} = \frac{\partial}{\partial x_j}\left[\left(\mathcal{T} + \mathcal{T}_t\right)\frac{\partial T}{\partial x_j}\right]$$

The thermal diffusivity of thermal and molecular thermal diffusivity are denoted by $\mathcal{T}$ and $\mathcal{T}_t$, respectively.

Using steady-state transport equations, the RNG K-ε turbulence model is used as:

$$\frac{\partial}{\partial x_j}(\rho \varepsilon u_i) = \frac{\partial}{\partial x_i}\left(\alpha_\varepsilon \mu_e \frac{\partial \varepsilon}{\partial x_i}\right) + C_1 \frac{\varepsilon}{k} G_k - C_2 \rho \frac{\varepsilon^2}{k}$$

$$\frac{\partial}{\partial x_j}(\rho k u_i) = \frac{\partial}{\partial x_i}\left(\alpha_k \mu_e \frac{\partial k}{\partial x_i}\right) + G_k - \rho \varepsilon$$

$$\mu_e = \mu + \rho C_u \frac{k^2}{\varepsilon}$$

The turbulent kinetic energy is denoted by K, the rate of dissipation by ε, and the effective viscosity by μe. We have defined k, ε, and μe using Eqs. 4, 5, and 6, respectively. where the values of the variables σε, σk, C1, C2, and Cu are 1.39, 1.39, 1.44, 1.92, and 0.0845, respectively.

Performance parameter evaluation

Finding out how well SAHs with VGs in corrugated plates handle hydraulics and heat is the driving force behind this research. The formulae below are used to compute the performance parameters:

Useful heat gains,

$$Q = \dot{m} C_p (T_o - T_i)$$

$$Re = \frac{\rho V D_h}{\mu}$$

Dh is the hydraulic diameter, and its formula is 4A/p. where A is the flow's cross-sectional area and p is the perimeter of the cross-wetted section.

The duct's internal pressure drop (Δp) is used to calculate the friction factor (f).

$$f = \frac{2\Delta P D_h}{4\rho L V^2}$$

Geometry description

The current study uses a finite volume numerical method to simulate "the flow of three-dimensional incompressible fluids" across a ribbed plate of a SAH that incorporates rectangular VGs. A three-dimensional SAH duct with measurements of 2500 mm × 300 mm × 50 mm for "length (L), width (w), and height (H)" was chosen as a result of the experimental work done by [19], as shown in Figure 2. Parts 800, 1200, and 500 mm in length make up the computational domain's three primary sections, which are the admission, test, and departure portions, respectively. The ASHRAE Standard is used to establish the lengths of the entry and exit components. The first part must be a minimum length of 5 (Width ~ Height)^0.5 and the other must have "2.5 (Width × Height)^0.5". It has experienced continuous change. While the solar duct's base and sides are entirely smooth, the test section's top surface—representing the absorber plate—is the only surface with rough edges. In order to induce turbulent flow in the test section, rectangular VGs having "angles of attack (α) of 30◦" were placed to the top wall of the entering component, as shown in Figure 1. Figure 1(b) illustrates the angle of attack, which is the angle formed between the vortex generator's chord line and the trajectory of the entering airflow. The dimensions of VGs are as follows: 60 mm for length, 25 mm for height, and 1.5 mm for thickness. In this study, there are 3 type of absorber plate design use to enhance the heat transfer. First is corrugated (wavy) shape, second is Triangular shape, and third is trapezoidal shape all are illustrated below. Vortex and SAH dimension and arrangement is constant in all design of SAH.

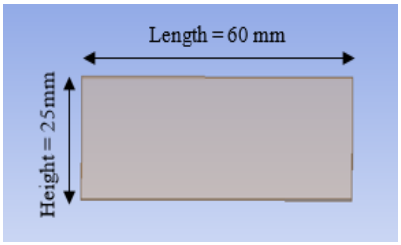

(a) Vortex generator design parameter

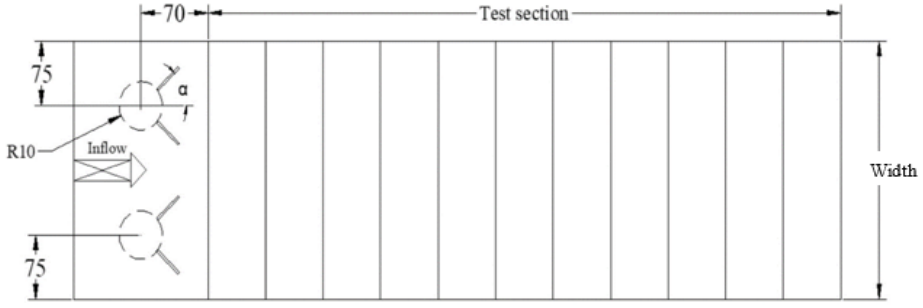

(b) Vortex generator arrangement

Figure 1 Vortex generator design parameter with solar air heater (SAH) duct

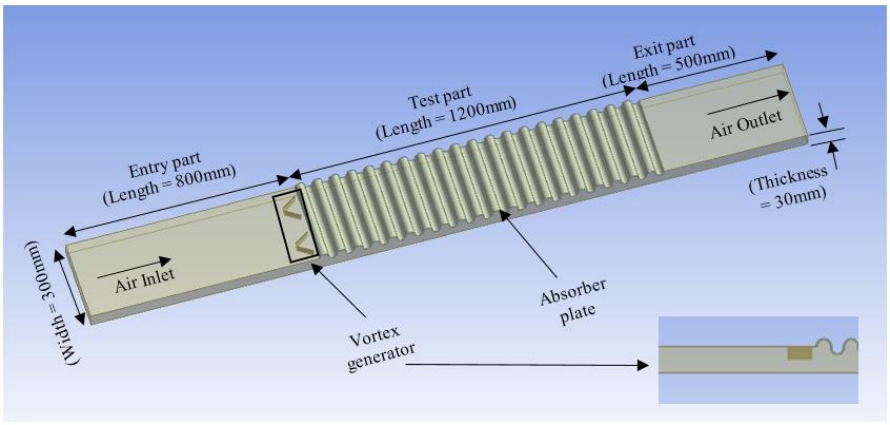

Figure 2 Design parameter of solar air heater duct

Design 1 (corrugated absorber)

Figure 3 shows the dimensions of the corrugated plate, which include its amplitude (4*R1) and wavelength (R1), with R1 set at 15 mm.

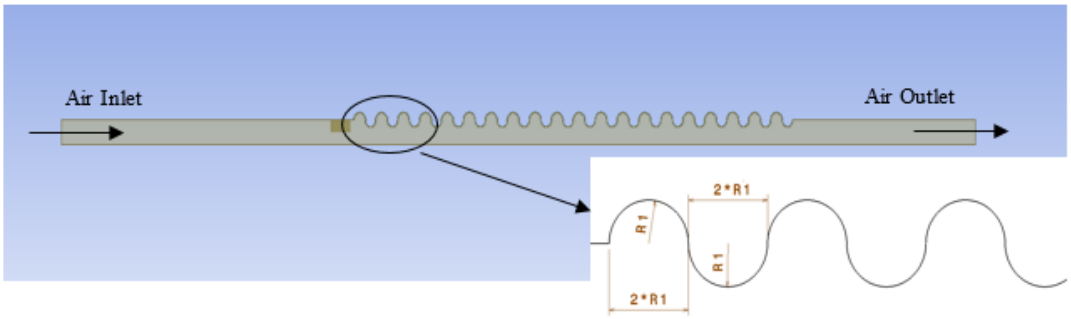

Figure 3 Design parameter of SAH with corrugated absorber plate

Design 2 (Triangular ribs)

Improved performance is achieved by upgrading the absorber plate of "the solar air heater" with triangular ribs. There are three different versions of the pattern, with varying rib counts. Each variation's rib count is determined by the triangular ribs' length. All versions of the triangle rib-shaped absorber plate with diverse rib length (L4) and rib height (h1), respectively. The specific details of the length, height, and number of ribs for each variation are summarized in the accompanying table 1, providing a clear comparison of the design parameters. This approach aims to optimise the heat transfer characteristics by methodically investigating the impact of rib shape.

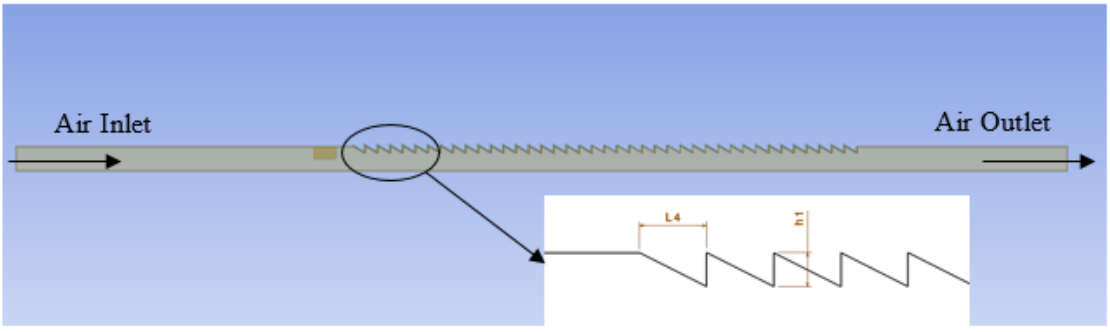

Figure 4 Design parameter of SAH with triangular rib series absorber plate

Table 1 Design notation and dimension of Triangular ribs shape absorber plate

Design notation	Length L4 (mm)	Height h1 (mm)	Number of ribs
Design 2-TN40	30	15	40
Design 2-TN80	15	10	80
Design 2-TN60	20	10	60

Design 3 (Trapezoidal ribs)

To improve heat transfer efficiency, this kind of solar air heater has a redesigned absorber plate that has multiple trapezoidal-shaped ribs. Two versions are included in the design, with the trapezoidal rib heights varying in each. While the heights of the ribs vary, the number of ribs and the rib length remain constant across all variations of this design. The lengths and heights of the ribs are denoted as L4, h1, and h2, respectively, for all configurations of the trapezoidal rib-shaped absorber plate.

Table 2 Design notation and dimension of trapezoidal ribs shape absorber plate

Design notation	Length L4 (mm)	Height (mm)		Length L5 (mm)	Pitch (mm)	Number of ribs
		h1	h2			
Design 3 – D10	15	10	5	23.7	8.7	51
Design 3 – D15	15	15	7	23.7	8.7	51

Additionally, as shown in Figure 5, the length L5 is defined as the sum of the rib length (L4) and the pitch, where the pitch is constant for all variations. The specific details regarding the rib length, pitch, heights (h1 and h2), and the number of ribs are outlined in the accompanying table 2. The impact of rib shape on the solar air heater's thermal efficiency may be easily investigated using this methodical approach to design.

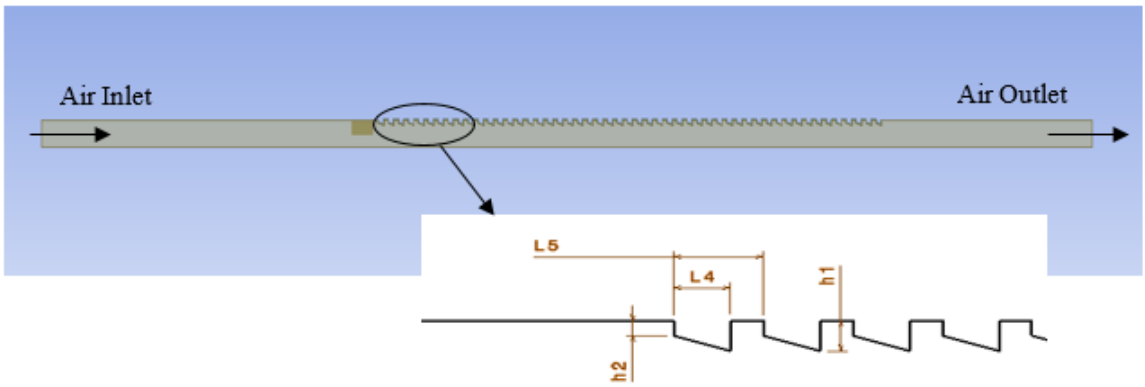

Figure 5 Design parameter of SAH with trapezoidal ribs absorber plate

Mesh generation

Due to its direct impact on the convergence and correctness of the findings, mesh creation is an essential stage in numerically simulating solar air heater ducts. The computational domain in this work was discretized using “hexahedral and tetrahedral mesh” components. The mesh element count and corresponding nodes for each design are summarized in a tabular format. Two methods were employed for mesh generation: body size and face size. For Design 1, featuring a wavy absorber plate, a body size of 0.02 mm and a face size of 0.03 mm were applied, ensuring a balanced representation of the complex geometry. In contrast, for Design 2 (triangular ribs) and Design 3 (trapezoidal ribs), the body size was set to 0.02 mm, while a finer face size of 0.01 mm was used to capture the intricate details of the ribbed surfaces. This approach allowed for efficient refinement of critical regions while maintaining computational feasibility. The combination of tetrahedral and hexahedral mesh elements provided flexibility in handling irregular geometries and ensured accurate resolution of flow and thermal gradients within the duct.

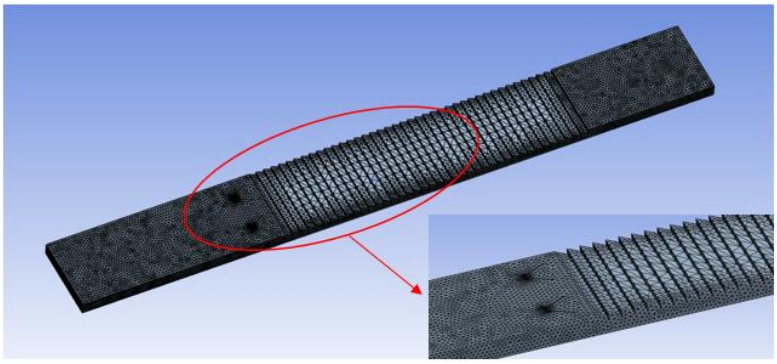

Figure 6 Meshing of SAH with various design of absorber plate

Table 3 Case notation and mesh element and nodes description

Cases	Design	Elements	Nodes
Case 1	Design 1- (Corrugated absorber)	643917	185100
Case 2	Design 2- TN40	135966	33300
Case 3	Design 2- TN80	141461	36074
Case 4	Design 2- TN60	138193	33863
Case 5	Design 3- D10	145259	38144
Case 6	Design 3- D15	146085	39467

Boundary condition

The current simulation study was carried out using the existing boundary conditions. Air is flowing inside the duct and the thermos-physical properties mention in the table. The initial air temperature and input velocity when fluid enters the duct are 300K and 1.31 m/s, respectively. At all times, 815 W/m2 of heat is flowing over the absorber plate's top surface. The side walls and base have been insulated.

Heat transfer and fluid flows were computationally simulated using a finite volume-based approach using the commercial software program ANSYS 23. The steady and incompressible flow settles the governing formulae and boundary conditions for momentum, energy, and continuity. "The semi-implicit method for pressure linked equation", or SIMPLE approach, is used to connect the pressure and velocity fields. The simulation is performed using a double-precision solver that is based on pressure. "A second-order up wind method" is used to discretize the governing formulas in space. The mesh tool and design modeller in ANSYS 23 are used to construct the geometry and mesh. The following values have been used as convergence criteria: 10−4 for "the rate of dissipation of turbulence, turbulence kinetic energy, and continuity"; 10−5 for velocity; and 10−8 for energy. The pressure and momentum under-relaxation parameters have been set at values of 0.3 and 0.7.

Table 4 Thermo-physical properties of air

Properties	Unit	Air
Density	Kg/m3	1.165
Specific heat capacity	J/kg*K	1007
Thermal conductivity	W/mK	0.0258
Viscosity	Pa-s	$1.87*10^{-5}$

Validation

The findings from [19] were compared and confirmed with the present numerical results for a corrugated absorber plate's frictional factor (f). A corrugated absorber panel with an amplitude of 15 mm and a wavelength of 60 mm was used in "a solar air heater (SAH) duct" to verify the results. Three portions, each measuring 800 mm, 1200 mm, and 500 mm, were separated into the SAH: the entrance part, the test part, and the departure part. As for the duct's dimensions, it was 300 mm wide and 50 mm high. An even 815 W/m² of heat flux was applied to the absorber plate's upper surface. The upper walls of the entry and exit portions, as well as "the bottom and side walls" of the duct, were completely

insulated. The air velocity in the duct was 1.31 m/s, and its temperature was 300 K. The current numerical results and those of [19] are contrasted in the figure 7. From the result comparison, an error of 8.7% was found between the two sets of results, indicating a minor discrepancy between the simulations. Despite this little disparity, the results demonstrate the value of the numerical approach used in this study.

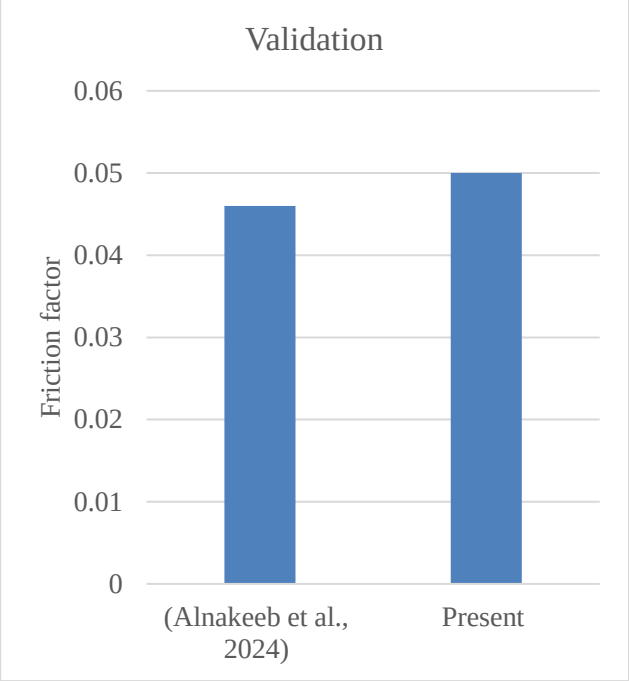

Figure 7 Validation graph

RESULT AND DISCUSSION

The impact of different absorber plate shapes is examined in this section along with the thermal and frictional characteristics of the airflow across "a solar air heater (SAH) duct". The results were compared using a corrugated absorber plate that had consistent heat flux and same flow parameters to evaluate the enhancement in "output temperature and heat transfer". The analysis highlights the behavior of airflow inside the SAH duct, considering variables such as temperature, pressure, and velocity. Specifically, the performance of corrugated, triangular rib, and trapezoidal rib absorber plates with vortex generators was examined, revealing significant differences in airflow characteristics within the duct.

Temperature distribution

Figures 8 illustrate the temperature distribution of airflow across different absorber plate shapes. The analysis considers two planes to evaluate the temperature distribution, which is represented by a color gradient ranging from 300 K to the maximum temperature achieved in each case. It is the same as the legend-shown maximum temperature for the absorber plate. The air's temperature starts to increase the moment it contacts the absorber plate. The inclusion of vortex generators alters the airflow path, diverting it in three directions: towards both corners and the middle region between the vortexes. This results in noticeable temperature increases at the corners and the central region of the duct.

In Case 1, as shown in Figure 4.1, the air temperature rises uniformly, with the entire airflow achieving a significant increase by the time it crosses the halfway point of the test section. The maximum air temperature in this case reaches approximately 338 K. In Case 2, depicted in Figure 4.2, the temperature rise begins after the air travels some distance within the test section. Case 3 follows a similar temperature distribution mechanism as Case 1 but achieves a higher maximum air temperature of approximately 357 K.

For Cases 4 and 5, the temperature distribution shows minor differences, as illustrated in Figures 4.4 and 4.5, indicating subtle variations in thermal performance. In Case 6, the temperature starts increasing immediately as the air enters the test section, with the highest temperature observed near the exit, reaching approximately 371 K. At the exit, the air temperature appears to stabilize, achieving equilibrium.

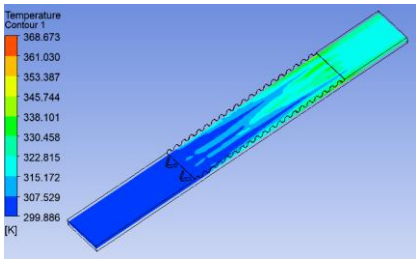

Case 1

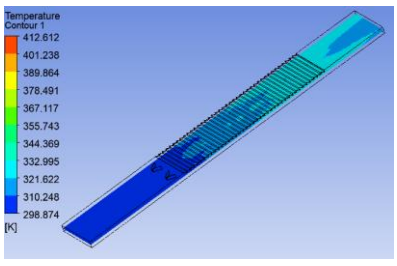

Case 2

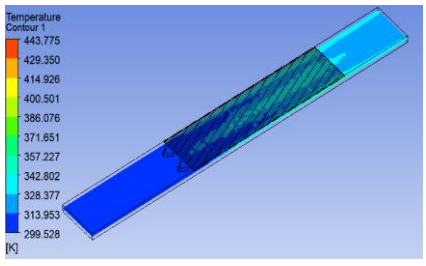

Case 3

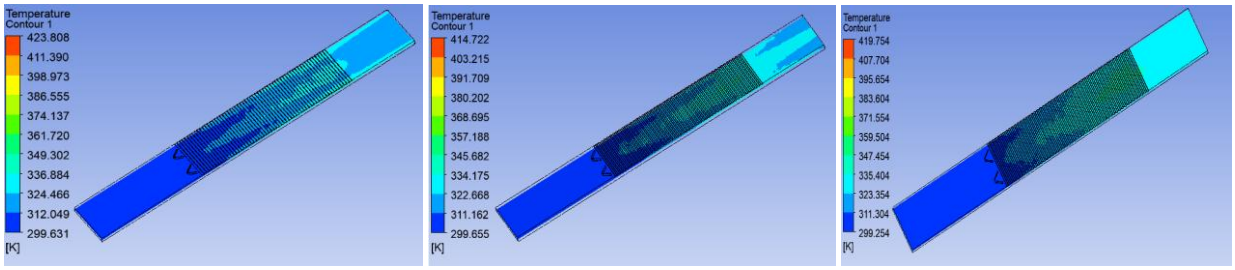

Case 4 Case 5 Case 6

Figure 8 Temperature distribution in all cases at horizontal plane

Pressure distribution

The pressure distribution in the airflow is depicted on a plane positioned at the mid-height of the duct. Figures 10 illustrate the pressure distribution for all cases, with values represented by a color gradient displayed on the left side of each figure. The pressure peaks at the duct's entrance portion, when airflow resistance is at its maximum. As the air travels through the test section, the pressure gradually decreases due to frictional and flow losses. By the time the airflow reaches the exit section, the pressure drops to its minimum or approaches zero.

The relationship between pressure and temperature is evident in the figures, as pressure is inversely proportional to temperature. This trend is particularly noticeable when comparing the pressure and temperature distribution figures, where regions of high temperature correspond to areas of low pressure. This behavior reflects the thermodynamic interplay between pressure and temperature in the airflow, highlighting the impact of heat transfer and flow dynamics within the duct.

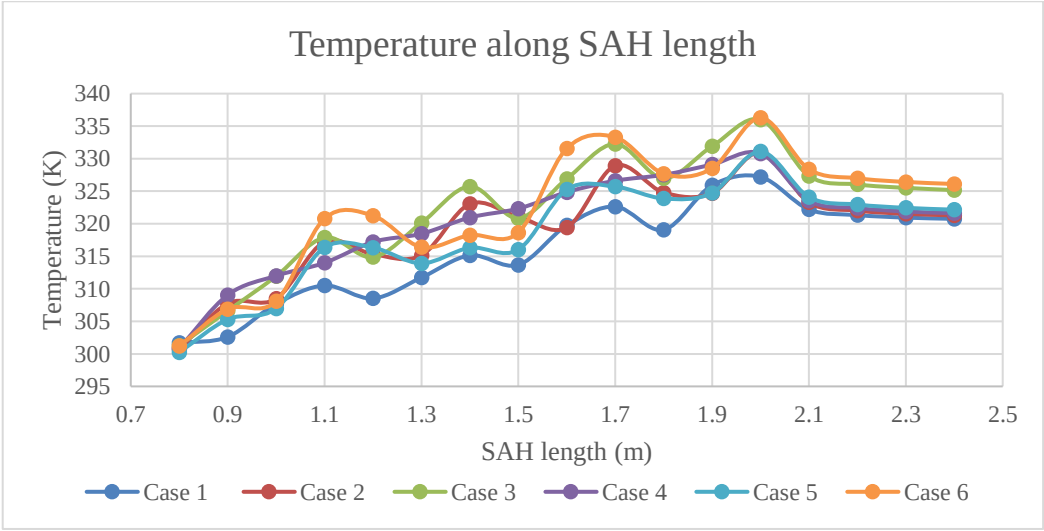

Figure 9 Average temperature along the length of SAH

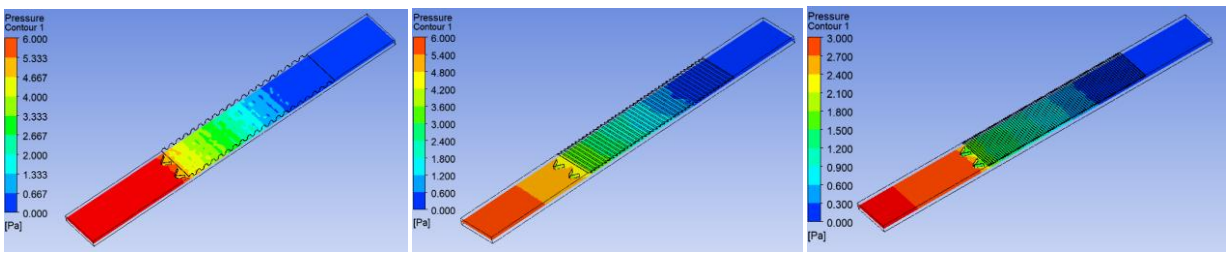

Case 1 Case 2 Case 3

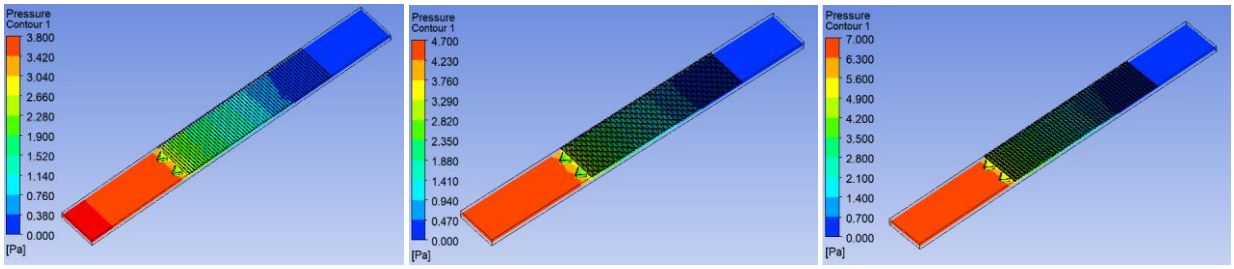

Case 4 Case 5 Case 6

Figure 10 Pressure distribution in all cases at horizontal plane

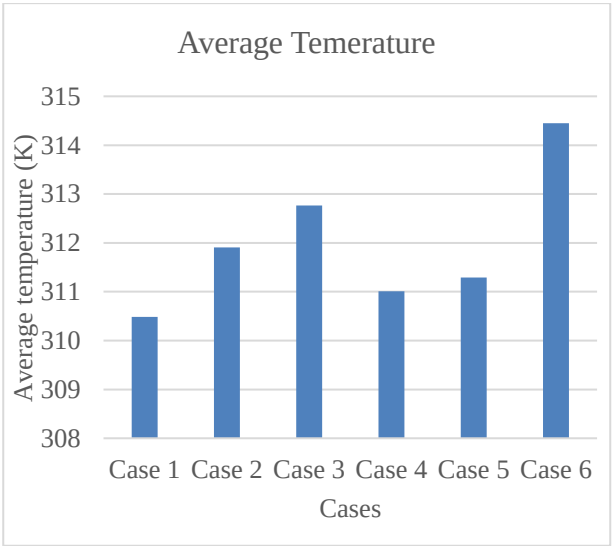

Figure 11 Average temperature in horizontal and vertical plane

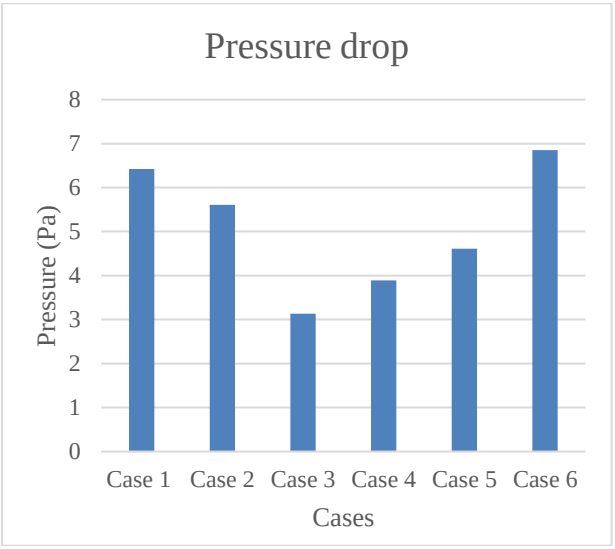

Figure 12 Pressure Drop In all cases

Velocity distribution

The three forms of the velocity distribution—two-plane distributions, and other is velocity streamlines,—are shown here. The volumetric depiction of airflow is shown by the velocity streamlines, which are lines that go from the duct's input to its output. The velocity magnitude is indicated by a color gradient displayed on the left side of each figure. The air's velocity rises when it engages with the "vortex generator" and further increases when it makes contact with the absorber plate.

In Case 1, the corrugated (wavy) absorber plate significantly enhances airflow velocity, reaching a maximum of 3.174 m/s along the lines generated by the vortex generator. The velocity becomes uniform near the exit section. In Case 2, the triangular rib absorber plate results in a lower maximum velocity of 2.263 m/s compared to Case 1. In this case, high velocity is observed near the vortex regions and along both side walls of the duct. Case 3 shows a further reduction in velocity, with a maximum of 2.146 m/s, due to modifications in the geometry of the triangular rib absorber plate. The maximum velocity is further reduced when the quantity of triangular ribs is increased but their height and length are decreased.

Case 4 shows a little decrease in velocity, which is explained by the absorber plate's longer and fewer triangular ribs. The maximum velocity in this case is 2.138 m/s, occurring near the vortex generator, along its line, and near the side walls of the test section. In Case 5, the use of a trapezoidal rib absorber plate causes an increase in maximum velocity, reaching 2.268 m/s. This increase is prominent near the vortex generator and the side walls of the test part. In Case 6, the maximum velocity rises further to 2.41 m/s due to an increase in the height of the trapezoidal rib structure on both sides. The highest velocities in this case are observed near the vortex generator and along the side walls of the test section.

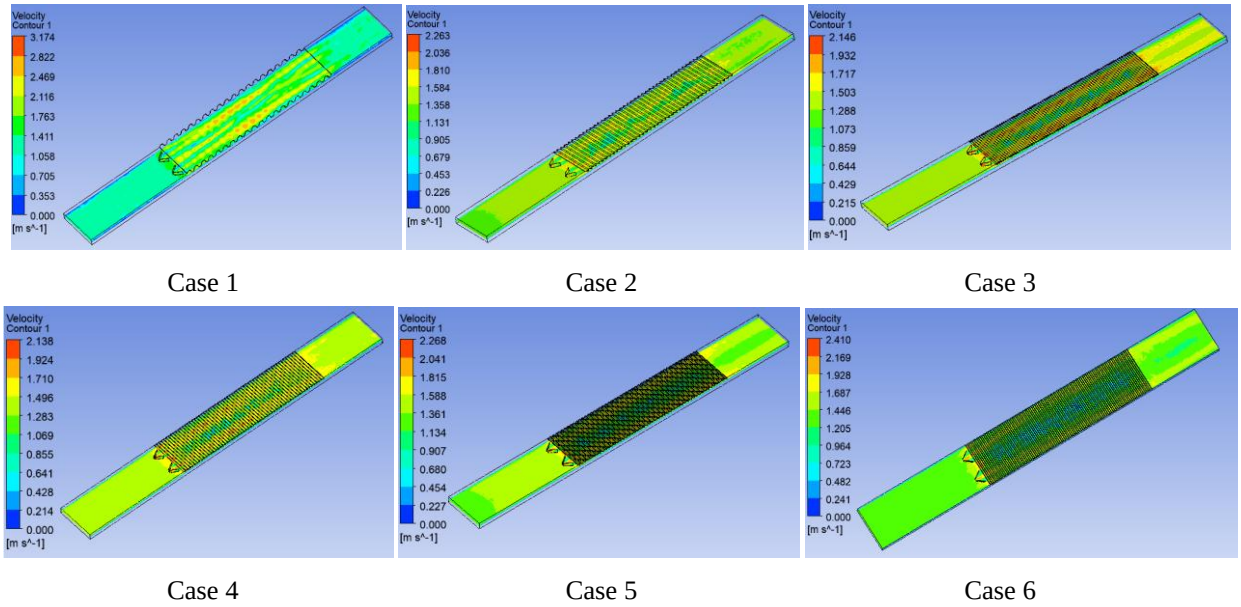

Figure 13 Velocity distribution all cases at horizontal plane

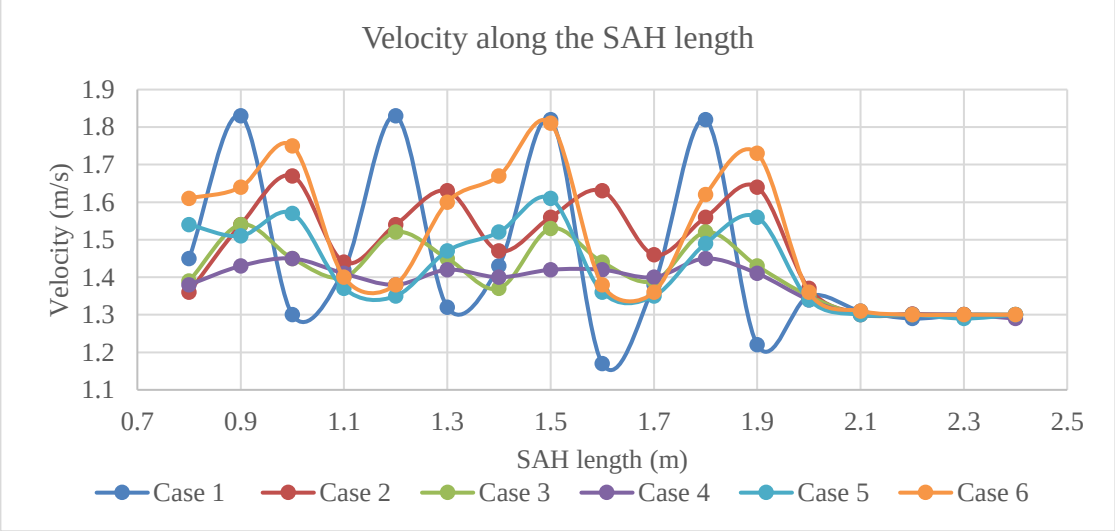

Figure 14 Average velocity along the SAH length

Outlet temperature

Case 1's solar air heater (SAH) achieves the lowest air temperature of 320.65 K using a corrugated absorber plate. Just after the airflow has gone through half of the test portion does the air temperature start to climb dramatically due to the corrugated plate's wavy configuration. A slightly higher output temperature of 321.15 K is achieved in Case 2 as a result of the elevated air temperature induced by the shape of the triangular rib absorber plate.

In Case 3, the triangular ribs' height and length are decreased, improving the airflow's ability to transfer heat. This modification results in a notable increase in the outlet temperature, reaching 325.14 K. Case 4 involves changes to the length of the triangular ribs, making their dimensions intermediate between those in Cases 2 and 3. Consequently, the outlet temperature also falls between these two cases, measured at 321.56 K.

Cases 5 and 6 employ trapezoidal rib absorber plates, differing primarily in the height of the trapezoidal ribs. In Case 5, the ribs have a lower height, resulting in an outlet temperature of 321.59 K. Conversely, in Case 6, the ribs are taller, which significantly enhances heat transfer and raises the outlet temperature to 325.83 K. Across all six cases, the maximum outlet temperature is achieved in Case 6, followed by Case 3, demonstrating the critical impact of rib geometry and dimensions on thermal performance.

Heat transfer

The amount of heat that a solar air heater can provide grows in proportion to the absorber plate's surface area that comes into contact with the air. The "rate of heat transfer" is directly proportional to the area of the absorber plate that comes into contact with the airflow. In Case 1, the corrugated absorber plate provides a contact area of 0.564 m², achieving a heat transfer rate of 475.99 W.

In Case 2, a triangular rib absorber plate is utilized, increasing the contact area to 0.583 m². The elevated heat transfer rate of 487.47 W is the end consequence of the enhanced performance. In Case 3, the number of triangular ribs is increased, further boosting the contact area to 0.673 m². The final outcome is a heat transfer rate of 579.52 W, which is an enormous improvement forward from the prior examples.

Case 4 features a reduction in the number of triangular ribs compared to Case 3, but still more than Case 2. With a constant air-to-absorber plate contact area of 0.583 m², 497.04 W of heat is transferred. Cases 5 and 6 employ trapezoidal rib absorber plates. In Case 5, the contact area is 0.602 m², leading to a heat transfer rate of 497.58 W. However, in Case 6, the trapezoidal ribs are designed with increased height, which maximizes the contact area to 0.727 m². This results in the highest heat transfer rate across all cases, measured at 595.44 W.

Among all the cases, Cases 3 and 6 exhibit the highest heat transfer rates, with Case 6 achieving the maximum value of 595.44 W, demonstrating the critical influence of rib geometry and contact area on thermal performance.

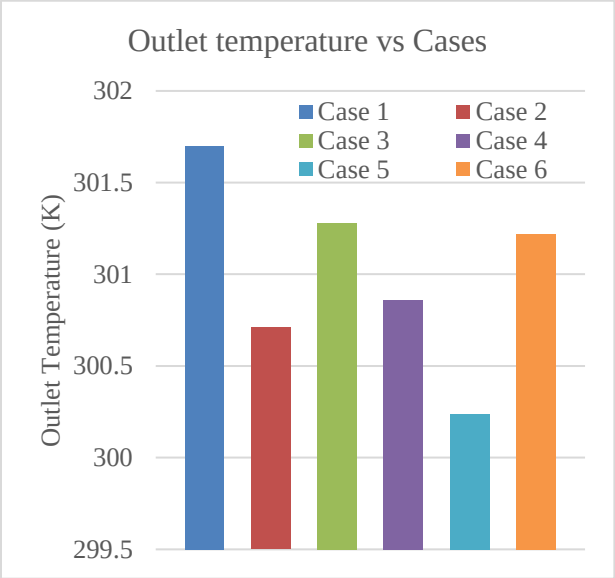

Figure 15 Outlet temperature comparison in all cases

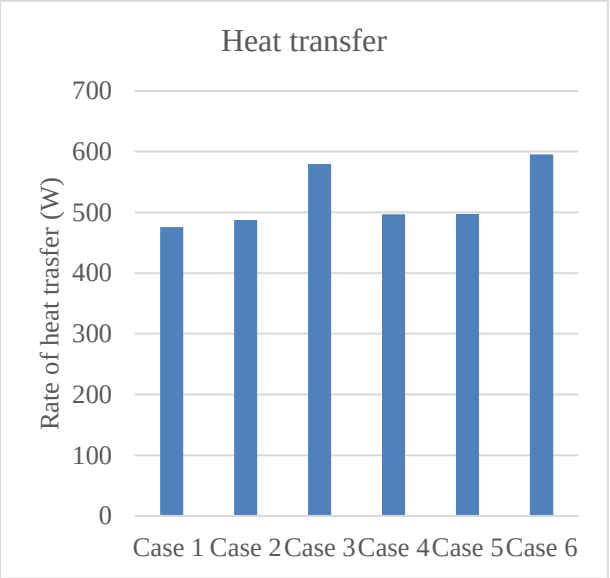

Figure 16 Rate of heat transfer in all cases

CONCLUSION

In this research, the main objective is to examine the effects of different absorber plate shapes. To transfer heat from the air to the plate, three distinct plate forms are utilised: corrugated, triangle, and trapezoidal. To improve heat transmission, several geometry adjustments are made for absorber plates with trapezoidal and triangular ribs. Six models were constructed using different absorber plate curvatures to maximize heat transmission in the SAH duct. From the simulation or investigation some outcomes describe below.

- There are two case having highest value in heat transfer and outlet temperature, which is case 5, &6.
- The value of heat transfer is directly related to the surface area of the absorber plate when it interacts with the air, as seen in the simulation.
- Highest pressure drop achieve in case 6 is 6.85 Pa.
- The outlet temperature of case 6 is 325.83 K, which is highest as compared to remaining other cases.
- The heat transfer of case 6, is 595.44 W, which is highest as compared to remaining other cases.

REFERENCES

[1] P. S. Pardeshi, M. Boulic, A. (Hennie) van Heerden, R. Phipps, and C. W. Cunningham, "Review of the thermal efficiency of a tube-type solar air heaters," *Renew. Sustain. Energy Rev.*, vol. 199, no. May, p. 114509, 2024, doi: 10.1016/j.rser.2024.114509.

[2] V. Singh, A. Singh, and A. Verma, "A Review on Experimental Analysis of Double Pass Solar Air Heater With Baffled Absorber Plate," *Int. J. Trend Sci. Res. Dev.*, vol. Volume-1, no. Issue-6, pp. 496–500, 2017, doi: 10.31142/ijtsrd3556.

[3] M. Assaye, M. Biadgelegn, and B. Fekadu, "Numerical investigation of convection heat transfer in solar air heater with semi-circular shape transverse rib," *Cogent Eng.*, vol. 9, no. 1, 2022, doi: 10.1080/23311916.2022.2106930.

[4] S. Li, H. Wang, X. Meng, and X. Wei, "Comparative study on the performance of a new solar air collector with different surface shapes," *Appl. Therm. Eng.*, vol. 114, pp. 639–644, 2017, doi: 10.1016/j.applthermaleng.2016.12.026.

[5] P. J. Bezbaruah, R. S. Das, and B. K. Sarkar, "Experimentally validated 3D simulation and performance optimization of a solar air duct with modified conical vortex generators," *Sol. Energy*, vol. 224, no. July, pp. 1040–1062, 2021, doi: 10.1016/j.solener.2021.06.052.

[6] H. Xiao, Z. Dong, Z. Liu, and W. Liu, "Heat transfer performance and flow characteristics of solar air heaters with inclined trapezoidal vortex generators," *Appl. Therm. Eng.*, vol. 179, no. January, p. 115484, 2020, doi: 10.1016/j.applthermaleng.2020.115484.

[7] S. S. Patel and A. Lanjewar, "Experimental investigation of solar air heater duct with discrete V-rib integrated with staggered elements," *Int. J. Sustain. Eng.*, vol. 14, no. 2, pp. 162–171, 2021, doi: 10.1080/19397038.2020.1737752.

[8] K. Almutairi, M. Alhuyi Nazari, M. Salem, M. M. Rashidi, M. El Haj Assad, and S. Padmanaban, "A review on applications of solar energy for preheating in power plants," *Alexandria Eng. J.*, vol. 61, no. 7, pp. 5283–5294, 2022, doi: 10.1016/j.aej.2021.10.045.

[9] V. P. Singh *et al.*, "Recent Developments and Advancements in Solar Air Heaters: A Detailed Review," *Sustain.*, vol. 14, no. 19, 2022, doi: 10.3390/su141912149.

[10] R. Shankar, R. Kumar, A. K. Pandey, and D. S. Thakur, "A comprehensive review of rectangular duct solar air heaters featuring artificial roughness," *Clean Energy*, vol. 8, no. 5, pp. 186–217, 2024, doi: 10.1093/ce/zkae063.

[11] P. K. Kannojia and R. Bahuguna, "Review Study on Solar Air Heater," vol. 3, no. 3, pp. 127–138, 2019.

[12] S. Panda and R. Kumar, "A Review on Heat Transfer Enhancement of Solar Air Heater Using Various Artificial Roughed Geometries," *J. Adv. Res. Fluid Mech. Therm. Sci.*, vol. 89, no. 1, pp. 92–133, 2022, doi: 10.37934/arfmts.89.1.92133.

[13] A. Elbrashy, F. Aboutaleb, M. El-Fakharany, and F. A. Essa, "Experimental study of solar air heater performance with evacuated tubes connected in series and involving nano-copper oxide/paraffin wax as thermal storage enhancer," *Environ. Sci. Pollut. Res.*, vol. 30, no. 2, pp. 4603–4616, 2023, doi: 10.1007/s11356-022-22462-6.

[14] N. K. Gupta, Karmveer, T. Alam, M. I. H. Siddiqui, R. Khargotra, and D. Dobrota, "A case study on thermal performance of solar air heater with down apex position of open trapezoidal ribs with gaps," *Case Stud. Therm. Eng.*, vol. 51, no. October, p. 103572, 2023, doi: 10.1016/j.csite.2023.103572.

[15] M. T. Baissi, A. Brima, K. Aoues, R. Khanniche, and N. Moummi, "Thermal behavior in a solar air heater channel roughened with delta-shaped vortex generators," *Appl. Therm. Eng.*, vol. 165, no. August 2018, p. 113563, 2020, doi: 10.1016/j.applthermaleng.2019.03.134.

[16] G. K. Chhaparwal *et al.*, "Numerical and experimental investigation of a solar air heater duct with circular detached ribs to improve its efficiency," *Case Stud. Therm. Eng.*, vol. 60, no. March, p. 104780, 2024, doi: 10.1016/j.csite.2024.104780.

[17] I. Singh, S. Singh, and S. Vardhan, "Heat transfer and fluid flow characteristics of solar air heater duct with non-uniform ribs," *J. Mech. Sci. Technol.*, vol. 35, no. 1, pp. 343–350, 2021, doi: 10.1007/s12206-020-1234-9.

[18] P. J. Bezbaruah, R. S. Das, and B. K. Sarkar, "Overall performance analysis and GRA optimization of solar air heater with truncated half conical vortex generators," *Sol. Energy*, vol. 196, no. December 2019, pp. 637–652, 2020, doi: 10.1016/j.solener.2019.12.057.

[19] M. A. Alnakeeb, M. A. Hassan, and M. A. Teamah, "Thermal performance analysis of corrugated plate solar air heater integrated with vortex generator," *Alexandria Eng. J.*, vol. 97, no. November 2023, pp. 241–255, 2024, doi: 10.1016/j.aej.2024.04.019.